UR-1211
ER-13065-663

Nucleon Structure Functions from ν_μ-Fe Scattering at the Tevatron*

The CCFR Collaboration
P.Z.Quintas, K.T.Bachmann [1], R.E.Blair [2], C.Foudas [3], B.J.King,
W.C.Lefmann, W.C.Leung, S.R.Mishra, E.Oltman [4],
S.A.Rabinowitz, F.J.Sciulli, M.H.Shaevitz, W.G.Seligman, W.H. Smith
Columbia University, New York, NY 10027
F.S.Merritt, M.J.Oreglia, B.A.Schumm
University of Chicago, Chicago, Il 60637
R.H.Bernstein, F. Borcherding, H.E.Fisk, M.J.Lamm,
H.Schellman, W.Marsh, K.W.B.Merritt, D.D.Yovanovitch
Fermilab, Batavia, IL 60510
A.Bodek, H.S.Budd, P.de Barbaro, W.K.Sakumoto
University of Rochester, Rochester, NY 14627

Presented by Arie Bodek, University of Rochester

ABSTRACT

We present preliminary results for nucleon structure functions measured in high energy neutrino interactions. Included are new results for the Gross-Llewellyn Smith Sum Rule, $\int \frac{1}{x} xF_3 dx = 2.66 \pm .03(\text{stat}) \pm .08(\text{syst})$, the ratio of cross-sections, $\sigma^{\overline{\nu}}/\sigma^{\nu} = .511 \pm .002(\text{stat}) \pm .005(\text{syst})$, and an analysis of the Q^2 evolution of xF_3.

1 Introduction

High energy neutrino interactions provide an effective way to measure the structure of the nucleon. The differential cross-section for charged-current interactions is:

$$\frac{d\sigma^{\nu(\overline{\nu})}}{dxdy} = \frac{G^2 s}{2\pi}\left[\left(1 - y - \frac{Mxy}{2E}\right) F_2(x,Q^2) + \frac{y^2}{2} 2xF_1(x,Q^2) \pm y(1-\frac{y}{2}) xF_3(x,Q^2)\right]. \quad (1)$$

By measuring the differential cross-sections for ν_μ-N and $\overline{\nu}_\mu$-N interactions, the structure functions F_2 and xF_3 can be extracted. These structure functions are related in the standard model to the momentum density of the constituent quarks, and are used to test both the quark-parton model and perturbative quantum chromodynamics (QCD).

---

[1]Present address: Widener Univ., Chester, Pa 19013.
[2]Present address: Argonne National Laboratory, Argonne, Il, 60439.
[3]Present address: Univ. of Wisconsin, Madison, Wi, 53706.
[4]Present address: LBL, Berkeley, Ca 94720.

*Presented at the IVth Conference on the Intersections Between Particle and Nuclear Physics, May 24-29, 1991, Tuscon, Arizona.

We present new high statistics, high energy data from the CCFR collaboration. The data were taken in two runs in the Fermilab Tevatron Quadrupole-Triplet Beam (QTB) with neutrino energies up to 600 GeV. A sample of 3,700,000 triggers was reduced after fiducial and kinematic cuts ($E_\mu > 15$ GeV and $\theta_\mu < .150$) to 1,281,000 ν- and 270,000 $\bar{\nu}$-induced events. This is an order of magnitude increase in statistics and a factor of two higher mean energy compared with the CCFR Narrow Band Beam (NBB) samples [1][2].

2 Calibration

The measurement of the structure functions depends critically upon understanding the energy resolution and calibration of the detector. The CCFR detector[3] consists of target calorimeter carts which measure hadron shower energy and muon angle followed by a toroid spectrometer which measures muon momentum. The polarity of the toroid was alternated during the running periods to take data both focusing and defocusing the muons. The detector was calibrated using charged particle test beams (independent of the neutrino running).

A hadron beam was directed into the target carts at different energies and different positions. The beam was momentum analyzed to high precision and had a narrow width (a few per cent). This data was used to calibrate the apparatus to better than 1% and determine the detector resolution function. Figure 1A shows the hadron beam data at one energy setting (100 GeV) and the parameterization obtained from the data.

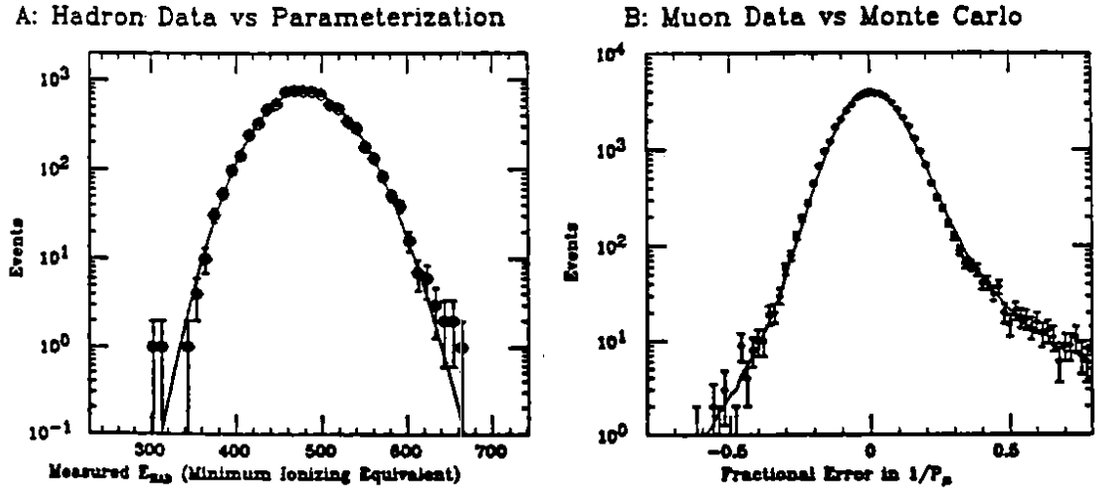

Figure 1: E_{had} and E_μ Resolutions

Muons from the test beam were used to calibrate the toroid spectrometer. Figure 1B shows the fractional difference in $1/P_\mu$ for data and Monte Carlo generated

events. The data is from one energy setting (120 GeV) of the test beam. The Monte Carlo calculation propagates the muon with full dE/dx loss (restricted and catastrophic energy losses: ionization, pair-production, and bremsstrahlung). Again the data and Monte Carlo match in mean as well as shape. Both the single-scatter and the catastrophic-loss tails are correctly modeled as well as the multiple Coulomb scattering which dominates the shape.

Certain aspects of the scaling violations are more sensitive to the difference in hadron and muon energy scales than to overall energy miscalibrations. The relative calibration of E_{had} to E_{μ} can be checked by plotting $\frac{<E_{vis}>^{DATA}}{<E_{vis}>^{MC}}$ as a function of $y = E_{had}/E_{vis}$. If the hadron and muon energy scales are the same, the ratio will be unity for all y. If not, the deviation of the slope from zero will measure the difference in energy scales. Figure 2 shows the relative calibration for focusing and defocusing events. Both are well within 1% of zero on average.

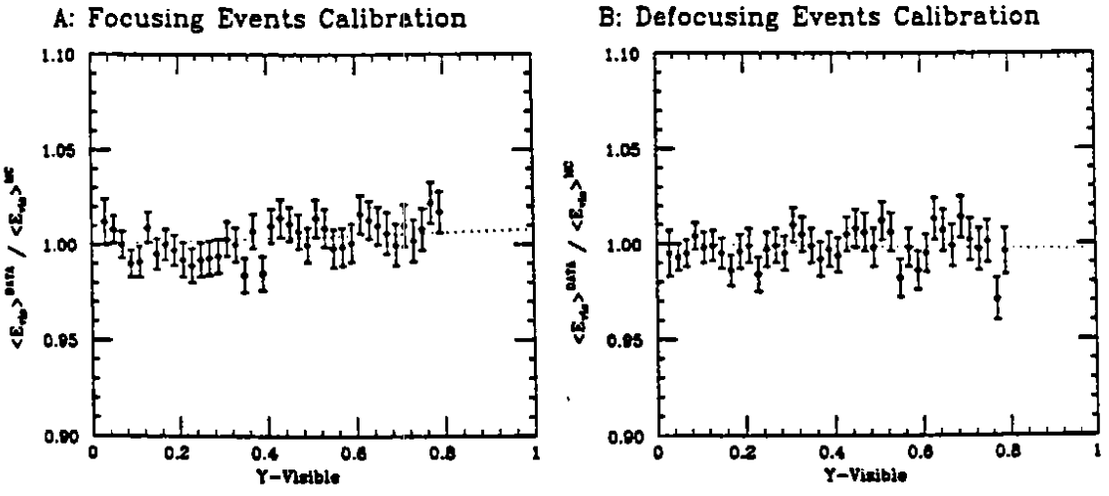

Figure 2: Relative Calibration for Focusing and Defocusing Events

3 Relative Flux Extraction

In the QTB there was no direct measurement of the secondary produced particles. Instead the neutrino flux had to be extracted from the charged-current data. From the events we can extract the relative flux, i.e. the ratio of fluxes at different energies and the ratio of neutrino to antineutrino flux. However, there is no direct measurement from this data of the absolute flux. Hence we normalize the data to the world average of the neutrino total cross-section in iron target experiments, $\sigma^{\nu N} = .68 \times 10^{-38}\, cm^2\, E_{\nu}(GeV)$[4][5].

The principal method of relative flux extraction used here is the fixed ν-cut method[6]. In the limit $y \rightarrow 0$ (or $\nu = E_{had} \rightarrow 0$), the differential cross-section

$d\sigma/d\nu$ approaches a constant which is independent of energy and the same for neutrinos and antineutinos. Thus after integration over all x and over ν from zero up to ν_0, the cross-section becomes independent of energy so that the relative flux is determined by counting events; i.e.

$$\Phi(E) \propto N(E, \nu < \nu_0) + \mathcal{O}(\frac{\nu_0}{E}) \tag{2}$$

where $\mathcal{O}(\frac{\nu_0}{E})$ indicates corrections of order ν_0/E arising from helicity induced y-dependent terms. The parameter ν_0 is chosen small enough to minimize corrections yet large enough to provide sufficient statistics. For our ν_0 cut of 20 GeV, there are 410,000 ν and 140,000 $\bar{\nu}$ events used for determining the relative flux.

Two other methods check the relative flux extraction. The first is the y-intercept method[7] which relies on the same principle but uses nearly the entire kinematic range. Events are binned at different energies as a function of y_{vis}. At each energy the value of the fitted intercept dN/dy at $y = 0$ is proportional to neutrino energy times flux. This method agrees with the fixed ν-cut method to 1.5%. The third method is the overlapping x and Q^2 bin method [1]. The structure functions calculated at different energies but in the same x and Q^2 bin should be equal. Applying this constraint provides another measure of the relative flux. The values so obtained agree with the fixed ν-cut flux to a few per cent.

The ratio of antineutrino to neutrino total cross-sections can be directly obtained, since the ratio of their fluxes is measured. This ratio is relatively free of systematic errors because it is a double ratio. The new data presented here include the first measurement of this quantity above 200 GeV (figure 3). The average over the energy range of 30–400 GeV is $.511 \pm .002(\text{stat}) \pm .005(\text{syst})$.

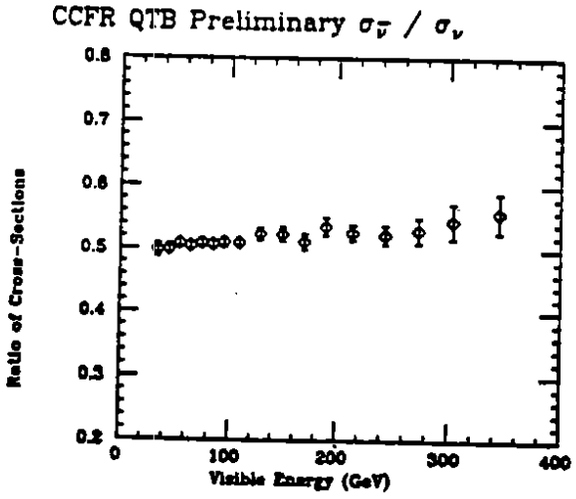

Figure 3: Ratio of Antineutrino and Neutrino Cross-sections

4 Structure Function Extraction

For the structure function analysis additional cuts of $E_{had} > 10$ GeV, $Q^2 > 1$ GeV^2, and $E_\nu > 50$ GeV were applied. After these cuts, there remained 990,000 ν- and 165,000 $\bar{\nu}$-induced events. The accepted events were separated into twelve x bins from .015 to .850 and sixteen Q^2 bins from 1 to 500 GeV^2. Eq. 1 takes the form

$$\frac{d\sigma^{\nu(\bar{\nu})}}{dxdy} = (a)F_2(x,Q^2) \pm (b)xF_3(x,Q^2) \tag{3}$$

after a number of assumptions discussed below. Integrating this cross-section times the flux over each x and Q^2 bin gives the number of events in that bin. We thus have sets of two equations in two unknowns to be solved for the structure functions at the bin centers, x_0 and Q_0^2.

$$\Delta N^\nu = (\int a\Phi(E)^\nu dE)(F_2(x_0,Q_0^2)) + (\int b\Phi(E)^\nu dE)(xF_3(x_0,Q_0^2)) \tag{4}$$

$$\Delta N^{\bar{\nu}} = (\int a\Phi(E)^{\bar{\nu}} dE)(F_2(x_0,Q_0^2)) - (\int b\Phi(E)^{\bar{\nu}} dE)(xF_3(x_0,Q_0^2)) \tag{5}$$

We assume $R \equiv \sigma^L/\sigma^T = R_{QCD}$ (the function predicted by pertubative QCD[8]). We apply corrections for the 6.85% excess of neutrons over protons in iron. We assume that the charm sea is zero and the strange sea is κ times the non-strange sea ($\kappa = .44$) [9]. We correct for threshold production of the heavy charm quark by the slow rescaling model[10][11] with $m_c = 1.31$ GeV[9]. Radiative effects follow De Rújula *et al.*[12], and the cross-section is corrected for the massive W-boson propagator.

5 Gross-Llewellyn Smith Sum Rule

The Gross-Llewellyn Smith Sum Rule[13] predicts that the integral of $\frac{1}{x}xF_3$ is the number of valence quarks in the nucleon. The value of three following from the naive parton model is modified by perturbative QCD and higher twist effects:

$$S_{GLS} \equiv \int \frac{1}{x}xF_3(x,Q^2)dx = 3\left[1 - \frac{\alpha_s(Q^2)}{\pi} + \mathcal{O}(\frac{1}{Q^2})\right] \tag{6}$$

The integral is evaluated at $Q^2 = 3$ GeV^2, which is the mean Q^2 of the lowest x bin, the bin which contributes most heavily to the integral. In each x bin a fit is made to $xF_3(x,Q^2)$ and interpolated or extrapolated to 3 GeV^2. These values of $xF_3(x,Q^2 = 3\text{ GeV}^2)$ are in turn fitted to $Ax^B(1-x)^C$ and this fit is integrated to determine the sum. The value obtained is $2.66 \pm .03(\text{stat}) \pm .08(\text{syst})$[14]. For $\Lambda = 250$ MeV the prediction for S_{GLS} is 2.63.

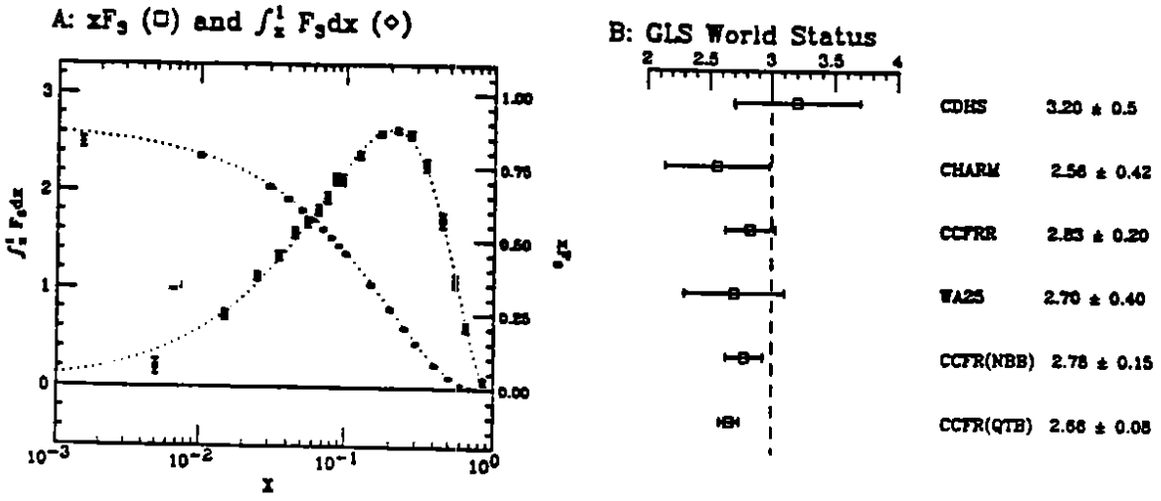

Figure 4: CCFR Preliminary GLS Measurement and World Status

Both the value of $xF_3(x, Q^2 = 3\ \mathrm{GeV}^2)$ (squares, right-side scale) and of the integral from x to 1 (diamonds, left-side scale) are shown in figure 4A. The results from this experiment and from previous ones [15] are illustrated in figure 4B. This new result is about a factor of two more precise than the previous best measurement of this quantity.

The overall error is small because of our good measurement at small x values. The systematic errors are dominated by the uncertainty in the overall level of the neutrino cross-section (2.2%), our measurement of the relative neutrino-antineutrino flux (1.5%), and the muon energy calibration (1.0%). The hadron energy and muon angle resolution uncertainties do not contribute significantly to the systematic error.

6 Structure Function Evolution

In pertubative QCD, structure functions are expected to evolve according to the equations

$$\frac{dF^{NS}(x,Q^2)}{dlnQ^2} = \frac{\alpha_S(Q^2)}{\pi}\int_x^1 P_{QQ}^{NS}(z)F^{NS}(\frac{x}{z},Q^2)dz \qquad (7)$$

$$\frac{dF^{S}(x,Q^2)}{dlnQ^2} = \frac{\alpha_S(Q^2)}{\pi}\int_x^1 (P_{QQ}^{S}(z)F^{S}(\frac{x}{z},Q^2) + P_{GQ}(z)G(\frac{x}{z},Q^2))dz \qquad (8)$$

where the P_{IJ} are the "splitting functions" predicted by the theory.

The non-singlet structure function (xF_3) evolution depends only on itself and the known splitting function. The singlet equation is more complicated: the evolution of F_2 is coupled with that of the gluons, $G(x)$. We only discuss the xF_3 evolution here.

The prediction for the slope (equation 7) involves a product of two terms, one of which depends on Λ_{QCD} (α_s) and one which does not (the integral). The splitting

function is independent of the value of the coupling constant to leading order so the behavior of the integral is known from the levels of the structure functions alone. The integral passes through zero at a point predicted by QCD, and hence the slope of xF_3 does so as well. Different values of Λ do not change this point but only vary the slope significantly when the integral is far from zero at high x. The low x behavior can be studied for consistency with QCD while the high x behavior provides the most sensitive measure of Λ. However the high x data points are also the most sensitive to the uncertainties in the energy scale and other systematic effects. Since our systematic studies are still in progress, we do not quote a value for Λ at this time.

The low x behavior is in itself quite interesting. There have been two previous measurements of the slope $\frac{dlnxF3}{dlnQ^2}$. For various values of Λ there exists a family of curves, all of which pass through zero at the same point and fan out at high x (figure 5A). The CDHS collaboration has provided high statistics data which are statistically inconsistent with the curves for all values of Λ [16]. The CCFR NBB data are too limited in statistics to be conclusive [2].

Figure 5B shows our new data along with a sample curve. We observe that our low x behavior agrees well with the QCD prediction. This observation is independent of the possible calibration adjustments and independent of the value of Λ. This is the first confirmation of the QCD prediction for a non-singlet structure function.

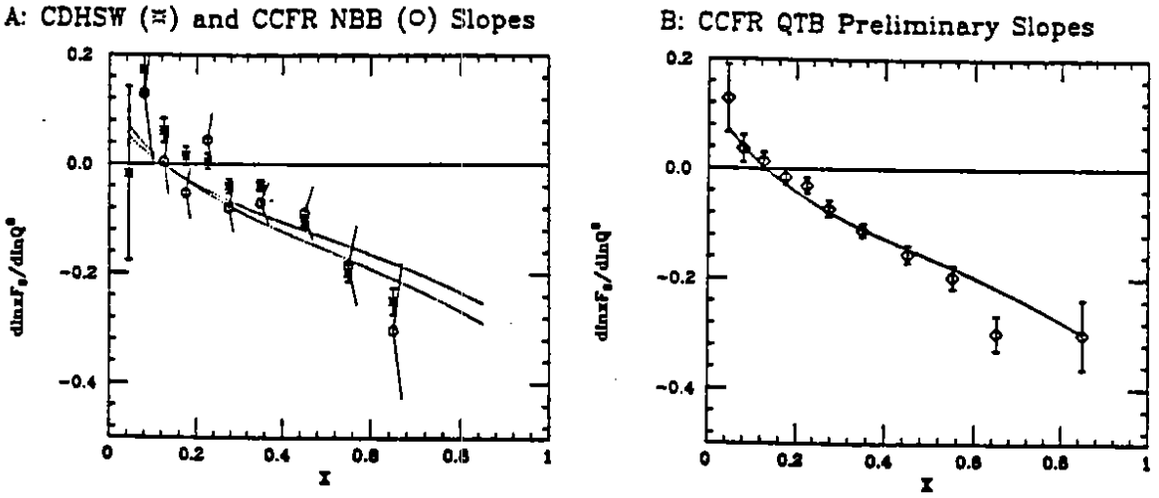

Figure 5: World Status and CCFR Preliminary xF_3 Evolutions

7 Conclusion

The CCFR collaboration has new high energy, high statistics structure functions. From this data we are able to extract the ratio of the neutrino and antineutrino cross-sections, $\sigma^{\overline{\nu}}/\sigma^{\nu} = .511 \pm .002 \pm .005$, the Gross-Llewellyn Smith Sum Rule,

$\int_0^1 \frac{1}{x} x F_3(x, Q^2 = 3\ \mathrm{GeV}^2) = 2.66 \pm .03 \pm .08$. The data also provide the first observation of the non-singlet structure function evolution consistent with QCD.

We acknowledge the gracious help of the Fermi National Accelerator Laboratory staff and the dedicated efforts of many individuals at our home institutions. This research was supported by the National Science Foundation and the Department of Energy.

References

[1] D.B.MacFarlane *et al. Z. Phys*, **C26**:1, 1984.

[2] E.Oltman. *Nucleon Structure Functions from High Energy Neutrino and Antineutrino interactions in Iron.* PhD thesis, Columbia Univ., 1989.

[3] W.K.Sakumoto *et al. UR-1142; to be published in NIM*, 1990.

[4] R.E.Blair *et al. Phys. Rev. Lett.*, **51**:343, 1983.

[5] P.Berge *et al. Z. Phys.*, **C35**:443, 1987.

[6] P.Z.Quintas *et al.* In preparation.

[7] P.S.Auchincloss. *NEVIS-1394; to be published in Z. Phys.*, 1990.

[8] G.Altarelli and G.Martinelli. *Phys. Lett.*, **76B**:89, 1978.

[9] C.Foudas *et al. Phys. Rev. Lett.*, **64**:1207, 1990.

[10] R.M.Barnett. *Phys. Rev. Lett.*, **36**:1163, 1976.

[11] H.Georgi and H.D.Politzer. *Phys. Rev. D*, **14**:1829, 1976.

[12] A.De Rújula *et al. Nucl. Phys.*, **B154**:394, 1979.

[13] D.Gross and C.Llewellyn Smith. *Nucl. Phys.*, **B14**:337, 1969.

[14] W.C.Leung *et al. Proceedings of the XXVth Rencontre de Moriond; NEVIS-1423*, 1990.

[15] S.R.Mishra and F.Sciulli. *Annu. Rev. Nucl. Part. Sci.*, **39**:259, 1989.

[16] B.Vallage. *Détermination Précise des Fonctions de Structure du Nucléon dans les Interactions de Type Courant-Chargé de Neutrinos sur Cible de Fer.* PhD thesis, L'Université de Paris-Sud, 1987.